

# From Compton scattering of photons on targets to inverse Compton scattering of electron and photon beams

Luca Serafini  and Vittoria Petrillo

*INFN Sez. Milano and Universita' degli Studi di Milano, Dipartimento di Fisica,  
Via Celoria 16, 20133 Milano, Italy*



(Received 2 May 2024; accepted 1 August 2024; published 28 August 2024)

We revisit the kinematics of Compton scattering (electron-photon interactions producing electrons and photons in the exit channel) covering the full range of energy/momenta distribution between the two colliding particles, with a dedicated view to statistical properties of secondary beams that are generated in beam-beam collisions. Starting from the Thomson inverse scattering, where electrons do not recoil and photons are backscattered to higher energies by a Lorentz boost effect (factor  $4\gamma^2$ ), we analyze three transition points, separating four regions. These are in sequence, given by increasing the electron recoil (numbers are for transition points and letters for regions): (a) Thomson backscattering, (1) equal sharing of total energy in the exit channel between electron and photon, (b) deep recoil regime where the bandwidth/energy spread of the two interacting beams are exchanged in the exit channel, (2) electron is stopped, i.e., taken down at rest in the laboratory system by colliding with an incident photon of  $mc^2/2$  energy, (c) electron backscattering region, where incident electron is backscattered by the incident photon, and (3) symmetric scattering, when the incident particles carry equal and opposite momenta, so that in the exit channel they are backscattered with same energy/momenta, and (d) Compton scattering [*à la* Arthur Compton, see A. J. Compton, A quantum theory of the scattering of X-rays by light elements, *Phys. Rev.* **21**, 83 (1923)], where photons carry an energy much larger than the colliding electron energy. For each region and/or transition point, we discuss the potential effects of interest in diverse areas, like generating monochromatic gamma-ray beams in deep recoil regions with spectral purification, or possible mechanisms of generation and propagation of very high energy photons in the cosmological domain.

DOI: [10.1103/PhysRevAccelBeams.27.080701](https://doi.org/10.1103/PhysRevAccelBeams.27.080701)

## I. INTRODUCTION

After the formulation of special relativity theory and the derivation of the relativistic Doppler effect [1], predicting a blueshift of e.m. field frequency seen by an observer in relativistic motion counter-propagating with respect to the direction of propagation of the electromagnetic (e.m.) wave (see Ref. [2]), confirmed by experimental measurements [3], the theoretical frame of classical electrodynamics was ready to explain and quantitatively calculate the characteristics of radiation generated by charged particles moving in space at relativistic velocities. Such a theoretical frame has been made available in the early 1900s by Einstein, Thomson, and Larmor, to predict a broad class of phenomena of radiation emission mechanisms where the quantum nature of e.m. fields was not

needed nor critical. Only after Compton's fundamental work [4], the quantum nature of e.m. fields, i.e., the photon, was experimentally demonstrated; its existence was a game changer and basically showed through Compton's measurements that the effect of electron recoil produced by the x-ray photon in the collision of x rays with atomic electrons could not be explained by classical electrodynamics and special relativity. The redshift of backscattered photons could be explained only invoking a photon-electron collision where the electron recoils and takes out some of the photon energy in the form of kinetic energy. After this discovery, the electron recoil became the fundamental parameter, i.e., the continental divide, between the classical picture of radiation emission and the quantum model of photon emission by charged particles propagating in space at relativistic velocities. In this paper, we revisit the full range of values that the recoil parameter can assume, from the very small values associated to Thomson scattering (or Thomson backscattering depending on the reference frame where the electron is observed) up to the deep recoil region, defined as when the incident photon has an energy much larger than  $mc^2$  in the electron rest frame, underlying four different domains and three transition points separating

---

*Published by the American Physical Society under the terms of the Creative Commons Attribution 4.0 International license. Further distribution of this work must maintain attribution to the author(s) and the published article's title, journal citation, and DOI.*

them. The recoil factor  $X$  is a dimensionless parameter given by

$$X = 4E_{\text{ph}}E_e/(mc^2)^2 = 4\gamma E_{\text{ph}}/mc^2 = 4\gamma^2 E_{\text{ph}}/E_e, \quad (1)$$

where  $E_e$  is the (total) electron energy and  $E_{\text{ph}}$  is the photon energy before the interaction, and the electron Lorentz factor  $\gamma$  is given by  $\gamma = E_e/mc^2$ . The recoil factor  $X$  is linked to the energy available in the center of mass reference system  $E_{cm}$  by  $E_{cm} = mc^2\sqrt{(1+X)}$ . The scope of this paper is to underline the specific behaviors and statistical properties of photon beams generated in correspondence of such transition points and regions. Several applications and investigation areas can benefit from these properties. We anticipate here the spectral purification mechanism active in the deep recoil region, the surprising property of x-rays with energy equal to  $mc^2/2$  to stop any colliding relativistic electron of any arbitrarily high kinetic energy, and the cancellation of the  $\gamma^2\theta^2$  angular correlation, inherent in any relativistic Doppler-based radiation source, occurring at the symmetric Compton scattering transition point [5]. Historically, the progress in understanding Compton scattering in its whole dynamical range, following the fundamental work of Compton, who studied the phenomenon in the frame of direct scattering of energetic (x ray) photons interacting with electrons at rest in the laboratory frame, has been initially pursued by researchers active in astrophysics, trying to explain the behavior of high energy charged particles propagating throughout the universe, interacting with photons of the cosmic background (microwave, infrared, and optical). Follin in 1947 first studied, in the course of his PhD thesis project [6], the inverse kinematics of a relativistic electron colliding with a low energy ( $< 1$  eV) photon where the term inverse defines a specular mode of interaction with respect to Compton's one, i.e., a configuration in the interaction where the photon gains energy in the collision at expense of the electron kinetic energy, the opposite of what happens in direct Compton scattering. Follin's study has been reissued 1 year later by Feenberg and Primakoff [7] still in the frame of astrophysical phenomena, where inverse Compton scattering plays a crucial role in determining the universe opacity to high energy photons and electrons.<sup>1</sup> Therefore, the first studies of inverse Compton scattering (ICS) dated back to the late 40s and had the aim to explain astrophysical phenomena related to the first observations of cosmic rays carried out just after the second World War. It has been only 15 years later, with the advent of high energy (GeV-class)

<sup>1</sup>Previous literature on inverse Compton attributed to Ref. [7], the first interpretation of inverse Compton—We discovered from Ref. 2 of Feenberg's paper that Follin developed and published his study 1 year earlier—Feenberg and his coauthor Primakoff were prompted by Oppenheimer to read Follin's work that anticipated their study.

electron synchrotrons and the invention of the ruby laser, that Milburn [8] first conceived the possibility to perform a laboratory-based experiment of ICS using the relativistic electron beams generated by particle accelerators making them collide with the intense optical photon beams made available by lasers. Milburn was quickly followed by Arutyunian and Tumanian's theoretical analysis [9]. The crucial role of recoil factor  $X$  was fully recognized since the initial stages of these theoretical studies, both in the astrophysical domain and in the accelerator-laser-based scenario; while in the astrophysical domain, Follin and Feenberg classified just two main regimes of the electron-photon collision kinematics, i.e., the low relativistic regime  $X \ll 1$  and the high relativistic regime  $X \gg 1$ , both accessible in the cosmic ray contest, Milburn and Arutyunian focused mostly on the low to mild relativistic regime ( $X < 1$ ) that was only accessible in laboratory experiments. The first measurements of ICS at a laboratory scale followed a few years after Milburn's publication at a number of particle accelerator laboratories [10–12]. We organize this paper as follows: In Sec. II, we discuss the full range of inverse kinematics reporting a synoptic table listing all ICS regions and transition points. In Sec. III, we show how the dependence on the collision angle is also vanishing in large recoil regimes, and in Sec. IV, we show some quantitative examples of spectral purification, the relevant aspect of large recoil electron-photon collisions, where the properties of the incident primary beams are mapped into the secondary beams with an exchange of entropy, i.e., the scattered photon beam is cooled and the exit electron beam after collision is heated, a strategic way to generate monochromatic gamma rays using monoenergetic incident electron beams and broadband white-spectrum photon beams. We should remark that in this paper, we are not discussing nonlinear effects due to intensity of the incident photon beam, i.e., those effects that become important when the laser parameter  $a_0$  associated to the optical photon beam carried by an incident laser pulse becomes close or larger than 1, inducing multiphoton or dressed-electron effects.

## II. DIFFERENT COMPTON SCATTERING REGIMES

In the synoptic Table I, the different Compton scattering regimes are summarized. Three transition points are listed in the table rows (namely, DICS, democratic inverse Compton scattering; FICS, full inverse Compton scattering; and SYCS, symmetric Compton scattering), separating four regions (namely, ITS, inverse Thomson scattering; DRCS, deep recoil Compton scattering; EBS, electron back scattering; and RDCS, relativistic direct Compton scattering), each characterized by specific range of collision kinematics. Table columns report all relevant parameters characterizing the electron-photon collision quantities: recoil factor  $X$ , energy of incident photon  $E_{\text{ph}}$ , maximum energy  $E'_{\text{ph}}$  of

TABLE I. Regimes of Compton scattering. ITS, inverse Thomson scattering; DICS, democratic inverse Compton scattering; DRCS, deep recoil Compton scattering; FICS, full inverse Compton scattering; EBS, electron backscattering; SYCS, symmetric Compton scattering; RDCS, relativistic direct Compton scattering.

Regime	Recoil factor	Incident photon energy	Maximum photon energy	Minimum electron energy	Center of mass energy	Electron rest frame
Symbol	$X$	$E_{\text{ph}}$	$E'_{\text{ph}}$	$E'_e$	$E_{cm}$	$E_{\text{ph}}^{\text{ERF}}$
Definition	$X = \frac{4\gamma E_{\text{ph}}}{mc^2}$	$k_x = k_y = 0$	$E'_{\text{ph}} = \frac{4\gamma^2 E_{\text{ph}}}{1+X}$		$E_{cm} = mc^2 \sqrt{1+X}$	$2\gamma E_{\text{ph}}$
ITS	$X \ll 1$	$\ll E_e$	$4\gamma^2 E_{\text{ph}}$	$\simeq E_e$	$\simeq mc^2$	$\ll mc^2$
DICS	$X = 1$	$\frac{mc^2}{4\gamma}$	$2\gamma^2 E_{\text{ph}}$	$2\gamma^2 E_{\text{ph}}$	$\sqrt{2}mc^2$	$mc^2/2$
DRCS	$1 \ll X \ll 2\gamma$	$\gg \frac{mc^2}{4\gamma}$	$\simeq (1 - \frac{1}{X})E_e$	$\ll E_e$	$> \sqrt{2}mc^2$	$> mc^2/2$
FICS	$X = 2\gamma$	$mc^2/2$	$E_e - mc^2/2$	$mc^2$	$\sqrt{2\gamma}mc^2$	$\gamma mc^2$
EBS	$2\gamma < X < 4\gamma^2$	$< \gamma mc^2$	$\sim E_e$	$< E_e$	$> \sqrt{2\gamma}mc^2$	$> \gamma mc^2$
SYCS	$X = 4\gamma^2$	$\gamma mc^2$	$E_{\text{ph}}$	$E_e$	$2\gamma mc^2$	$2\gamma^2 mc^2$
RDCS	$X > 4\gamma^2$	$> \gamma mc^2$	$< E_{\text{ph}}$	$> E_e$	$> 2\gamma mc^2$	$> 2\gamma^2 mc^2$

scattered photon at  $\theta = 0$  scattering angle (full backscattering), the corresponding minimum energy  $E'_e$  of the scattered electron, the energy in the center of mass reference frame  $E_{cm}$ , and the energy of the incident photon as seen in the electron rest frame  $E_{\text{ph}}^{\text{ERF}}$ . Note that the incident electron is assumed to be relativistic (i.e.,  $\gamma \gg 1$ ) and the electron-photon collision is assumed to be head-on (i.e., vanishing transverse momentum of the incident photon and electron). Furthermore, all calculations have been done with a relative bandwidth of the initial photons  $bw_{\text{ph}} = 5\%$ . Besides the recoil factor  $X$ , a second dimensionless parameter governing the kinematics of Compton scattering is the asymmetry parameter  $A$ , defined as in Ref. [5]:

$$A = \gamma^2 - X/4 = (E_e - E_{\text{ph}})E_e/(mc^2)^2 \quad (2)$$

(in case of relativistic electrons).  $A$  represents the divide between direct Compton scattering (characterized by  $A < 0$ , where the energy of the incident photon is larger than the energy of the incoming electron), and inverse Compton scattering (region defined by  $A > 0$ ) where the electron energy before interaction is larger than that of the incident photon.  $A = 0$  is the transition point where the scattering is fully symmetric (actually the center of mass reference system is steady in the laboratory system because the total momentum is null) and was denominated symmetric Compton scattering in Ref. [5].

For simplicity in the discussion, we will consider in this section an ideal head-on collision between an electron of energy  $E_e$  and momentum aligned with the  $z$  axis, directed toward positive  $z$ , and a photon of energy  $E_{\text{ph}}$ , counter-propagating with respect to the electron toward negative  $z$ . The generalization to an arbitrary value of the collision angle  $\alpha$  between the incoming electron and the incident photon will be given in Sec. III. The electron momentum before collision is  $\mathbf{P} = (p_x = 0, p_y = 0, p_z = \beta\gamma mc)$ , while the photon momentum is  $\hbar\mathbf{k} = (\hbar k_x = 0, \hbar k_y = 0, \hbar k_z = -E_{\text{ph}}/c)$ . Following Refs. [13,14] and invoking

the conservation of total energy and momentum, the scattered photon energy  $E'_{\text{ph}}$  will be given by the well-known formula:

$$E'_{\text{ph}} = E_{\text{ph}} \frac{\gamma^2(1 - \beta \cos \alpha)}{\gamma^2(1 - \beta \cos \theta) + \frac{X}{4}[1 - \cos(\alpha + \theta)]}, \quad (3)$$

where  $\alpha$  is the interaction angle between the incoming electrons and photons, and the scattered photons are propagating at a scattering angle  $\theta$  with respect to the  $z$  axis. If electron and photons are counterpropagating ( $\alpha = \pi$ ), then the previous equation reduces to:

$$E'_{\text{ph}} = \frac{(1 + \beta)E_{\text{ph}}E_e}{(1 - \beta \cos \theta)E_e + (1 + \cos \theta)E_{\text{ph}}} \quad (4)$$

that is valid for any arbitrary value of colliding electron and photon energy and momentum. Actually, the direct Compton effect is represented by Eq. (3) [or Eq. (4), if  $\alpha = \pi$ ] just setting  $\beta = 0$  and  $E_e = mc^2$  that applies to an electron at rest in the laboratory system. In this way, Eq. (3) transforms into the well-known Compton's formula:

$$E'_{\text{ph}} = \frac{E_{\text{ph}}}{1 + (1 + \cos \theta)E_{\text{ph}}/mc^2}. \quad (5)$$

By knowing the value of the scattered photon energy  $E'_{\text{ph}}$ , and calling  $E_{\text{tot}} = E_e + E_{\text{ph}}$ , it is straightforward to derive the electron energy after scattering as  $E'_e = E_e + E_{\text{ph}} - E'_{\text{ph}} = E_{\text{tot}} - E'_{\text{ph}}$ . Nevertheless, our focus is on relativistic electrons, so Table I illustrates the behavior of electron and photon energies after scattering in case  $\gamma \gg 1$ . Therefore, the fourth region named RDCS (namely, relativistic direct Compton scattering) refers to direct Compton effect with electrons in relativistic motion in the laboratory system, though of energy smaller than that of incident photons. In order to better illustrate the four regions and three transition points of

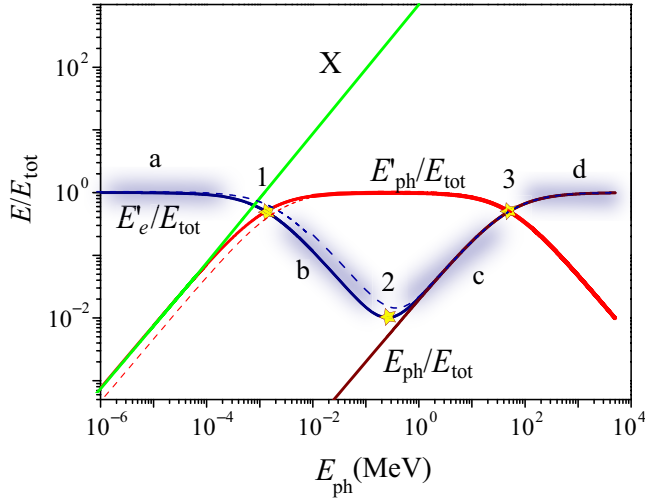


FIG. 1. Different regimes of emission versus the initial photon energy (in MeV) for  $E_e = 50$  MeV. All energies, namely,  $E'_e$  (in blue),  $E'_{ph}$  (in red), and  $E_{ph}$  (in black) are dimensionless, normalized to  $E_{tot}$ . The recoil  $X$  (on the same left ordinate) is in green. Yellow stars indicate points, and shaded strips indicate regions. (a) indicates the regime ITS, (b) indicates DRCS, (c) EBS and (d) RDCS; (1) represents the point DICS, (2) represents the point FICS, and (3) SYCS. Dashed curves are scattered photons evaluated at an observer angle  $\theta = 1/\gamma$  and the relevant scattered electrons.

generalized Compton scattering, we specialize in the following the discussion considering those photons that are totally backscattered and propagate at a scattering angle  $\theta = 0$  after colliding with the electron. These are photons achieving maximum energy gain or loss depending on the value of the asymmetry parameter  $A$  (photons gain energy when  $A > 0$  and lose energy when  $A < 0$ ). If  $\theta = 0$ , the energy of the backscattered photon is simply given by  $E'_{ph} = 4\gamma^2 E_{ph}/(1+X)$ . We plot in Fig. 1, the relevant quantities characterizing the kinematics as a function of the incident photon energy  $E_{ph}$  for a fixed incident electron energy, namely  $E_e = 50$  MeV. All energies are normalized to the total energy of the system  $E_{tot} = E_e + E_{ph}$ . The recoil parameter  $X$  is also plotted. The normalized energies of the electron and photon after scattering can be expressed in terms of only the recoil parameter  $X$  and the Lorentz factor  $\gamma$  as follows:

$$\frac{E'_{ph}}{E_{tot}} = \frac{X}{(1+X)(1+\frac{X}{4\gamma^2})}, \quad (6)$$

$$\frac{E'_e}{E_{tot}} = 1 - \frac{X}{(1+X)(1+\frac{X}{4\gamma^2})}. \quad (7)$$

These are very useful expressions to explain how to classify the various regimes and transition points of Compton inverse-direct scattering. In the picture is also

presented, in dashed lines, the energy of the emitted photons at angle  $\theta = 1/\gamma$  and the correspondent electrons, showing that at large recoil factor the energies are substantially invariant with the scattering angle. Figure 2 shows the total momentum  $p_{tot}$  as well as the final electron and photon momenta, respectively,  $p'_e$  and  $p'_{ph}$ . The first region, named inverse Thomson scattering [label (a) in Figs. 1 and 2], is basically defined as that of “negligible momentum exchange” between the incident photon and the colliding electron: as a matter of fact that the momentum exchange in the electron rest frame (ERF) is given by  $2E_{ph}^{ERF} = 4\gamma E_{ph}$  (note that  $X = 2E_{ph}^{ERF}/mc^2$ ). If the momentum exchange is negligible with respect to  $mc^2$ , then the condition  $X \ll 1$  holds, and the backscattered photon in ERF will have same energy as  $E_{ph}^{ERF}$ : Lorentz transforming back to the laboratory system will give  $E'_{ph} = 2\gamma E_{ph}^{ERF} = 4\gamma^2 E_{ph}$ . Hence, inverse Thomson scattering can be simply explained as inverse photon scattering with negligible momentum exchange (note that in this regime the total energy-momentum conservation is violated by the expression  $4\gamma^2 E_{ph}$  unless  $X \ll 1$ ). ITS regime and its peculiar  $4\gamma^2$  scaling of the backscattered photon energy can be also explained going through a classical electrodynamics description of undulator radiation emitted by the electron oscillating in the em. field of the counter-propagating laser pulse (see Ref. [15]). The majority of inverse Compton sources under design or operation belong to this ITS regime (see [16]), with the exception of XFELo ([17]). Looking at Eqs. (6) and (7), it is interesting noticing that the two particles after scattering have equal energy, i.e.,  $E'_e = E'_{ph}$  when the recoil parameter becomes equal to either  $X = 1$  or  $X = 4\gamma^2$ . We denominate the transition point characterized by  $X = 1$ , labeled (1) in Figs. 1–3, democratic inverse Compton scattering, since the two particles emerging after scattering are sharing democratically the total energy of the system  $E_{tot}$  and the total momentum  $p_{tot}$  [while before scattering most of the energy is carried by the electron and the photon carries an energy still much smaller than  $mc^2$ , namely  $mc^2/(4\gamma)$ ]. The second solution  $X = 4\gamma^2$ , which is valid only when  $\gamma \gg 1$ , corresponds actually to symmetric Compton scattering, very well discussed and analyzed in Ref. [5], which is characterized by interacting electron and photon carrying equal energy and momentum before and after scattering. In SYCS [point (3) in the figures] what happens is basically a flip-over of the incoming momentum of the two scattering particles, that just flip the direction of their momentum without modifying their energy, with a uniform angular distribution after scattering. Region (b) in Figs. 1 and 2, denominated deep recoil Compton scattering, is characterized by an increasing value of the recoil factor, in the range  $1 \ll X \ll 2\gamma$ . In this region, the incident electron is going to lose most of its energy/momentum in favour of the backscattered photon: a saturation effect starts to appear

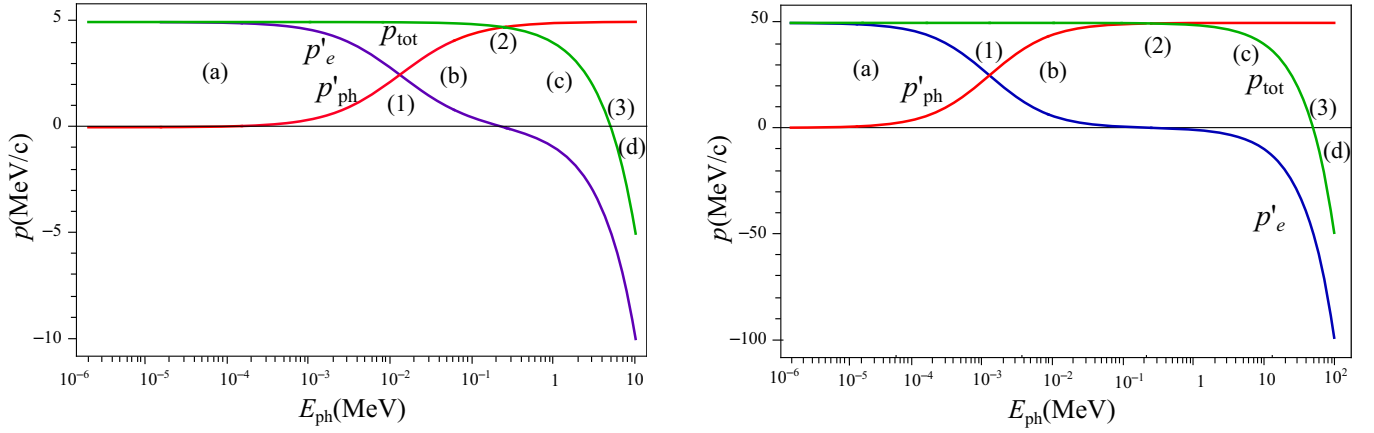


FIG. 2. Momenta versus the initial photon energy (in MeV) for left  $E_e = 5$  MeV and right  $E_e = 50$  MeV. All momenta (namely  $p'_e$  (in blue),  $p'_ph$  (in red), and  $p_{tot}$  (in green) are in MeV/c. (a) indicates the regime ITS, (b) indicates DRCS, (c) EBS and (d) RDCS; (1) represents the point DICS, (2) represents the point FICS, and (3) SYCS.

the energy of the backscattered photon, given approximately by  $(1 - 1/X)E_e$ , which depends only perturbatively on the energy of the incident photon (through the recoil factor  $X$ ). This is the basis of spectral purification mechanism that is further discussed in Sec. IV. Still in region (b), the scattered electron emerging after scattering keeps propagating toward the incidental positive  $z$ -axis direction, as clearly shown in Fig. 2. Instead, in region (c), denominated electron backscattering, characterized still by a large value of the recoil factor, the electron starts to be backscattered and propagating back in the negative direction of the  $z$  axis after scattering. Both in region (b) and region (c), the emerging photon after scattering is carrying almost all the total energy of the system, since  $E'_{ph}/E_{tot} \simeq 1$ .

This is the region denominated “extremely relativistic” in Refs. [7] and [9], whose authors discuss the amount of energy lost by the electron in a single collision. The electron loses a large fraction of its kinetic energy in favour of the photon when collisions take place in regions (b) and (c). The way inverse Compton scattering in deep recoil regime can be realized is doublefold. Either considering electrons with increasing initial energy  $E_e$  before scattering, as in Refs. [7,9] (dealing with astrophysical phenomena where incident photons are in the microwave or infrared or optical range), or increasing the energy of the incident photon, as discussed here. What matters in order to keep  $X$  large is the product of the incident photon energy and the incoming electron energy: just as a side comment we note that the maximum value achieved in experiments operated in laboratories with accelerators, has been about  $X = 1.9$  so far (see Ref. [18], reporting the data of experiment E144 at SLAC) using about 45 GeV electron beams colliding with IR (1.2 eV photons) and green (2.4 eV photons) laser pulses—DICS has been observed in a single-photon linear Compton scattering in this experiment, as clearly reported in the photon spectra published in this paper. There is, however, a special transition point,

denominated full inverse Compton scattering [point (2) in Figs. 1–3], that is characterized by a unique absolute value of the incident photon energy, i.e.,  $E_{ph} = mc^2/2$ , which is the divide between electrons emerging after scattering with still positive momentum [regions (a) and (b)] and electrons backscattered with negative momentum [region (c) and (d)] by the collision with incident photons. At the FICS transition point, the electron is taken down to rest in the laboratory system by the interaction with a 255.5 keV ( $mc^2/2$ ) photon; its energy after scattering is just  $mc^2$ . Its kinetic energy is totally transferred to the backscattered photon that will propagate back toward positive  $z$ -axis direction with energy  $E'_{ph} = E_e - mc^2/2 = T_e + mc^2/2$ . Interesting to note that  $mc^2/2$  is a value playing an important role also in direct Compton scattering, with a dual behavior than FICS: as a matter of fact if we consider an incident photon on a target, as predicted by Eq. (5), with an energy much larger than the electron rest mass energy, i.e.,  $E_{ph} \gg mc^2$ , then the backscattered photon at  $\theta = 0$  will have an energy equal to  $E'_{ph} = mc^2/2$  independently on the energy  $E_{ph}$  of the incident photon. At FICS point, the recoil factor is  $X = 2\gamma$ . We believe that FICS can play an important role in astrophysical gamma-ray sources, where the flux of 255.5 keV x rays can be intense and can interact with very high energy electrons generating in turns very high energetic photons in a single collision with extremely large energy transfer. At the end, FICS is the Compton scattering modality maximizing the energy/momentum transfer from the electron to the photon; this characteristic was not specifically underlined in the previous literature. The impressive characteristic of FICS interaction point is the capability of 255.5 keV photons to stop “any” relativistic electron of whatsoever energy. Figure 3 shows that the different emission regimes for  $E_e = 50$  MeV.  $E'_e$  (in blue),  $E'_{ph}$  (in red), and  $E_{ph}$  (in black) in MeV are represented versus  $E_{ph}$  in MeV. The stars

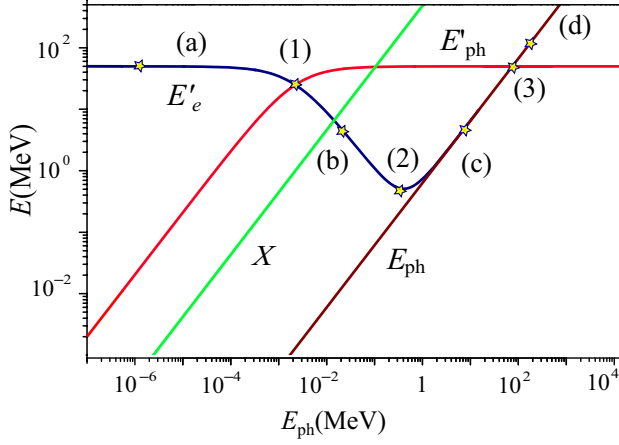


FIG. 3. Different regimes of emission versus the initial photon energy (in MeV) for  $E_e = 50$  MeV.  $E'_e$  (in blue),  $E'_ph$  (in red), and  $E_{ph}$  (in black) in MeV are represented versus  $E_{ph}$  in MeV. The recoil  $X$  (on the same left ordinate) is in green. Differently from Fig. 1, the quantities (except  $X$ ) are not dimensionless. The stars represent the values chosen for the spectrum simulations.

represent few typical values chosen for spectral simulations. In Table II, the values assumed by some relevant quantities are reported. Figures 4–6 show both the total radiation spectrum, i.e.,  $\frac{dN'_{ph}}{E'_{ph}}$  versus  $E'_{ph}$  ( $N'_{ph}$  being the number of emitted photons collected in the whole solid angle) and the electron energy distribution versus  $E'_e$ , in various situations. The first of these points falls in the inverse Thomson scattering regime (a 50 MeV electron beam collides with an optical radiation pulse of 1.5 eV energy) and is an example of the various Compton sources operating worldwide [16]. Characterized by a small recoil  $X = 1.1 \times 10^{-3}$ , this working point generates hard x rays of edge energy  $E'_{ph} = 57.4$  keV, in a range useful for medical imaging applications.

The total radiation spectrum, shown in Fig. 4, window (i) in red, has the typical bowl shape, while the electrons (in blue) lose in the interaction a negligible amount of energy. The emitted photons are all in the  $1/\gamma$  cone, while the electrons maintain their straight trajectories.

When the recoil is  $X = 1$ , corresponding to  $E_{ph} = 1.3$  keV for  $E_e = 50$  MeV [Fig. 4, window (ii)], the emitted photon and the emerging electron spectra maintain the broad bowl shape, while the Compton edge and the minimum electron energy limit coincide at about  $E = E_e/2$ . The photon angular distribution still covers the  $1/\gamma$  aperture and the emerging electrons are all close to the axis. Increasing further the recoil, penetrating the deep recoil regime (DRS), [see Fig. 4, window (iii)], the radiation spectrum develops a sharp forward peak, already described in Refs. [14,17]. In a symmetric way, the electrons lose energy. The angular distributions begin to enlarge. This situation achieves its maximum expression in correspondence to the full inverse Compton scattering (FICS) point, where the electron beam, hit by photons at 255.5 keV, stops whatever its energy. As shown in the simulation (Fig. 5), there is an almost full exchange of energy between the photons and the electrons. The photon spectrum appears strongly peaked at the initial electron energy at 50 MeV, while the electrons lose almost all their kinetic energy, stabilizing at 511 keV total energy  $E'_e$ . While the photons still propagate in a cone around the positive  $z$  axis, the electrons scatter in the whole solid angle and a consistent fraction revert. Increasing the incoming photon energy beyond 255.5 keV [Fig. 6, windows (i), (ii), and (iii)], the emitted photon energy remains attested at the initial electron energy value (namely 50 MeV), the remaining energy being acquired by the electrons which now move faster and faster in the reverse direction. The radiation spectrum shrinks, reaching the full monochromaticity in correspondence of the symmetric inverse Compton scattering (SYCS) point [6, window (ii)], defined by the condition  $E_e = E_{ph}$  and widely analyzed in Ref. [5] also in general to nonrelativistic electrons, for which the SYCS condition actually applies to the electron and photon momentum, i.e.,  $p_e = \hbar k$ . We note that a relatively broad bandwidth of the initial photon beam does not change the thinness of the final spectrum. In Fig. 6, the initial photon relative bandwidth is assumed 5%, while in the symmetric Compton condition, the final bandwidth is under 0.2%. Conversely, the electrons, even if monoenergetic at the beginning, exit the collision

TABLE II. Parameters of simulations:  $E_e$ , initial electron energy;  $E_{ph}$ , initial photon energy;  $bw_{ph}$ , relative bandwidth of the initial photons;  $X$ , recoil factor; and  $A$ , asymmetry factor.

Regime	$E_e$	$E_{ph}$	$bw_{ph}$	$X$	$A$	Max scatt. ph. En.	Min scatt. e-En.	Cent. of mass En.	Figure
						MeV	MeV	MeV	
ITS	50	$1.5 \times 10^{-6}$	5	0.0011	9574	0.057	50	0.511	Fig. 4
DICS	50	$1.3 \times 10^{-3}$	5	1	9574	24.88	24.88	0.722	Fig. 4
DRCS	50	$10^{-2}$	5	7.65	9572	43.46	6.5	1.5	Fig. 4
FICS	50	0.2555	5	195.7	9525	50	0.2555	7.1	Fig. 5
EBS	50	15	5	$1.15 \times 10^4$	6700	50	15	54.7	Fig. 6
SYCS	50	50	5	$3.8 \times 10^4$	74	50	50	99.99	Fig. 6
RDCS	50	150	5	$1.15 \times 10^5$	-9676	50	150	173	Fig. 6

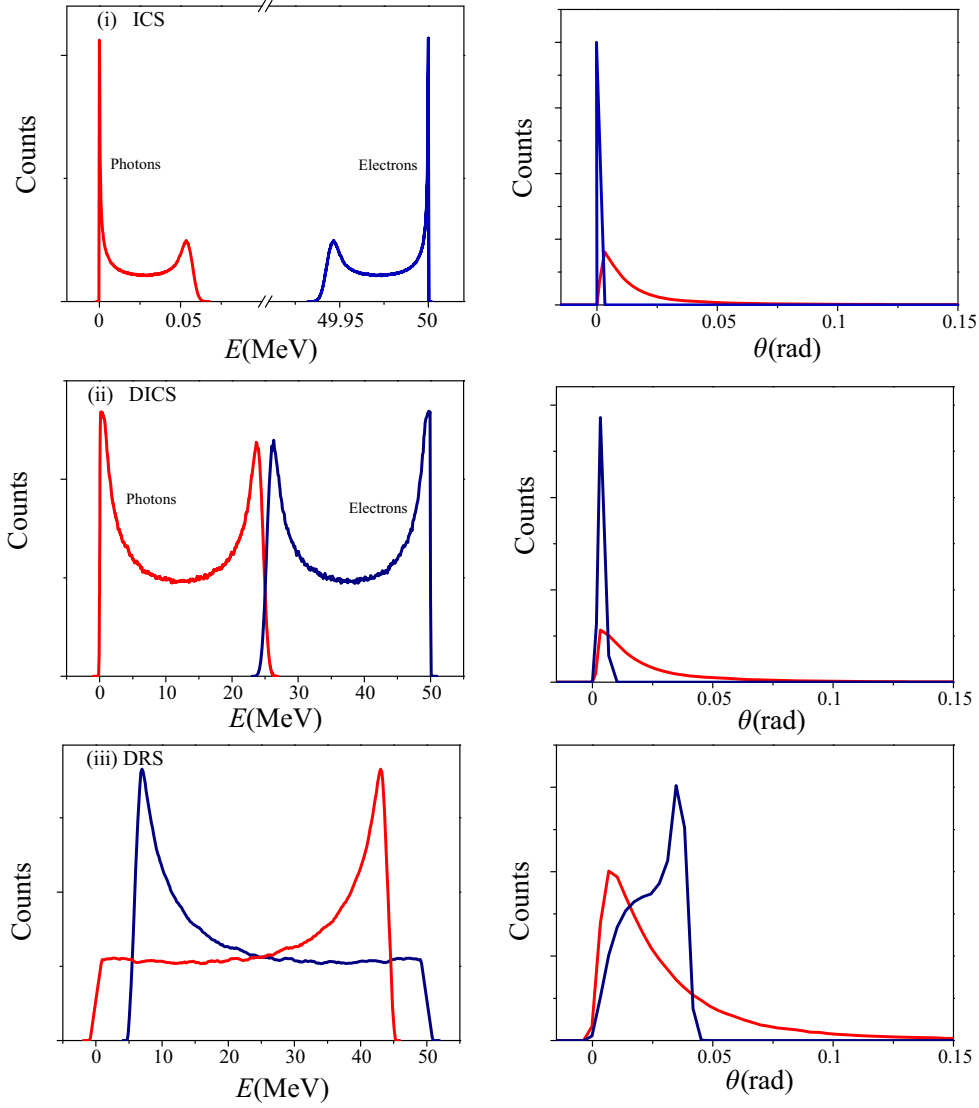


FIG. 4. (i) Inverse Thomson scattering (ITS). Left: energy distribution, right: angular distribution. Red: scattered photons, blue: scattered electrons.  $E_{\text{ph}} = 1.5$  eV,  $E_e = 50$  MeV, and  $bw_{\text{ph}} = 5\%$ . (ii) Democratic inverse Compton scattering (DICS).  $E_{\text{ph}} = 1.3$  keV,  $E_e = 50$  MeV, and  $bw_{\text{ph}} = 5\%$ . (iii) Deep recoil scattering (DRS).  $E_{\text{ph}} = 10$  keV,  $E_e = 50$  MeV, and  $bw_{\text{ph}} = 5\%$ .

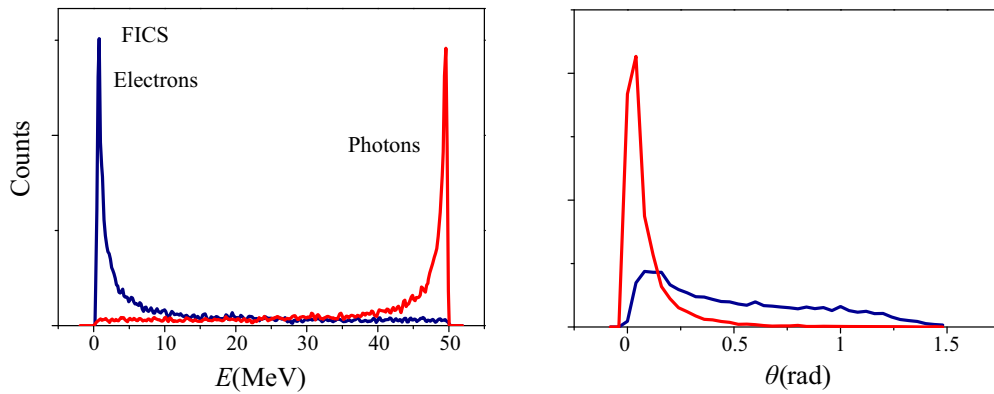


FIG. 5. Full inverse Compton scattering (FICS). Left: energy distribution, right: angular distribution. Red: scattered photons, blue: scattered electrons.  $E_{\text{ph}} = 255.5$  keV,  $E_e = 50$  MeV, and  $bw_{\text{ph}} = 5\%$ .

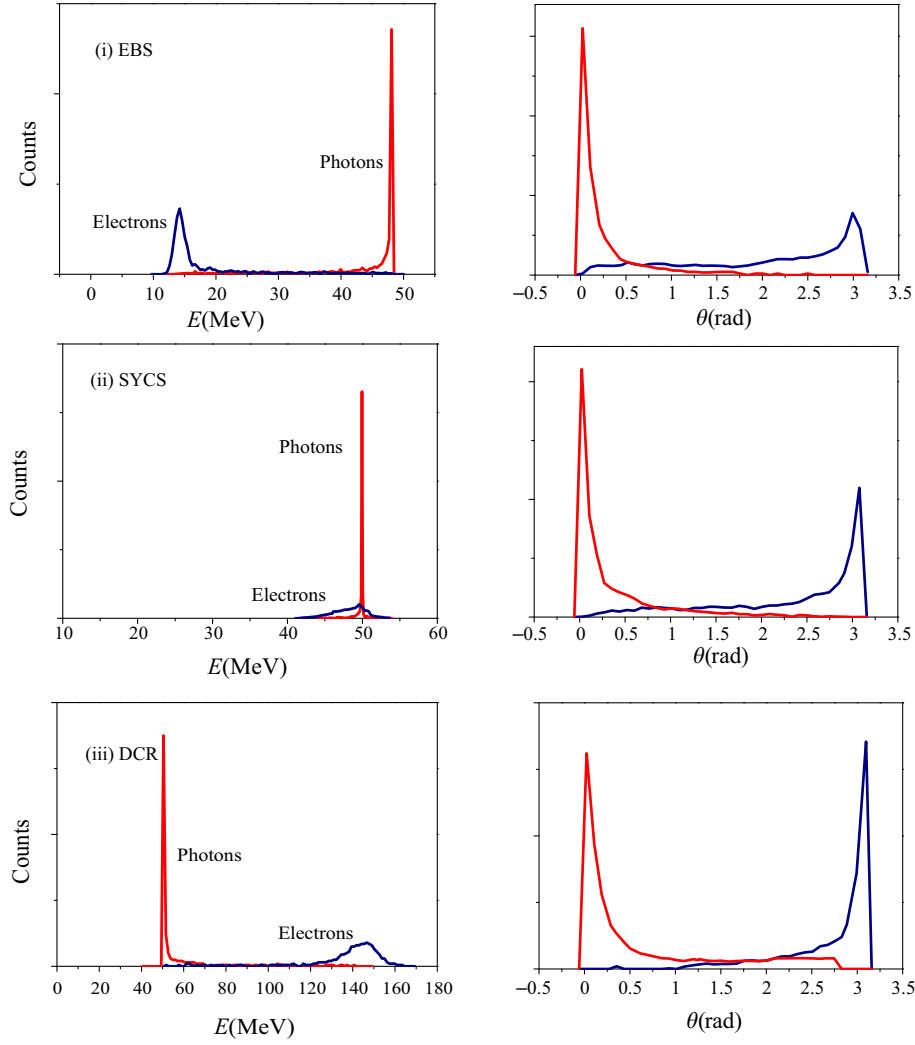


FIG. 6. (i) Electron backscattering (EBS). Left: energy distribution, right: angular distribution. Red: scattered photons, blue: scattered electrons.  $E_{\text{ph}} = 15$  MeV,  $E_e = 50$  MeV, and  $bw_{\text{ph}} = 5\%$ . (ii) Symmetric Compton scattering (SYCS):  $E_{\text{ph}} = 50$  MeV,  $E_e = 50$  MeV, and  $bw_{\text{ph}} = 5\%$ . (iii) Relativistic direct Compton scattering:  $E_{\text{ph}} = 150$  MeV,  $E_e = 50$  MeV, and  $bw_{\text{ph}} = 5\%$ .

dispersed in energy. As explained in Ref. [7] (see equation 31), and also discussed in Refs. [13] and [14], when the recoil factor  $X$  is very large (and in case shown in Fig. 5, the recoil factor is  $X = 195.7$ ) the bandwidth of the incident photon beam is damped by a factor  $1/(1+X)$  onto the bandwidth of the scattered photons. So the result shown in Fig. 5 is basically insensitive to the bandwidth  $bw$  of the incident photon beam. We considered  $bw = 5\%$  just as a reference value, but we checked the Monte Carlo code outputs generated using  $bw = 0.3\%$  (as typical of a Yb:Yag laser beam used for interaction) and the spectra are not different from those shown in Fig. 5.

The unbelievable properties of the FICS working point are highlighted in Fig. 7. Spanning a very large range of incident photon energies, from 1  $\mu\text{eV}$  up to 1 TeV (in order to cover the energy range of intragalactic and extragalactic photon background, spanning from CMBR to EBL and ISRF, see Ref. [19]), and considering interacting electron

energies of 100 GeV, 1, 10, 100 TeV, and 1, 100 PeV, all curves plotted in Fig. 7 show the energy of the electron after scattering  $E'_e$ . This quantity exhibits a common minimum at  $mc^2/2$  incident photon energy with a common value of  $E'_e = mc^2$  independent on the initial electron energy  $E_e$ . It is also interesting to notice that the behavior of  $E'_e$  as function of  $E_{\text{ph}}$  becomes independent on the initial electron energy  $E_e$  as soon as the recoil factor  $X$  becomes much larger than 1, as well shown in Fig. 7. This is clearly due to the fact that for large recoil the energy of the backscattered photon asymptotically tends to the energy of the incident electron, therefore,  $E'_e$  asymptotically tends to  $E_{\text{ph}}$ . Nevertheless, we need to underline that increasing the energy available in the center of mass  $E_{cm}$ , as clearly inherent in data shown in Fig. 7, other reactions become competitive and statistically more likely than Compton scattering, like triplet production (above  $E_{cm} = 1.5$  MeV), muon pair production (above  $E_{cm} = 210$  MeV), and other



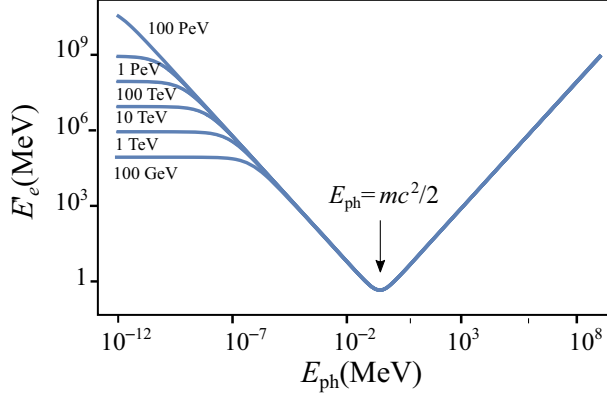


FIG. 7.  $E'_e$  as a function of  $E_{\text{ph}}$  for various values of initial energy  $E_e$ , namely 100 GeV, 1, 10, 100 TeV, 1, and 100 PeV. Note that all electrons stop after collision when  $E_{\text{ph}} = mc^2/2 = 0.2555$  MeV, independently on their initial energy  $E_e$ . The incident photon energy region  $E_{\text{ph}} = 10^{-10}$  to  $10^{-9}$  MeV corresponds to the cosmic microwave background radiation (CMBR), while the region  $E_{\text{ph}} = 10^{-7}$  to  $10^{-5}$  MeV corresponds to extragalactic light (EBL) and interstellar radiation field (ISRF), Ref. [19].

hadronic reactions involving pion/meson production, which become dominant only above  $E_{cm} = 600$  MeV (see Ref. [20]), which implies  $E_e = 360$  GeV for 255.5 keV incident photons. A specific discussion on cross section behaviors of different QED processes in this energy range can be found in Ref. [21]. The behavior shown in Fig. 7 is strictly relative to the kinematics of inverse Compton scattering in exotic regions of the incident particle energy range never considered previously in the literature under such specific details. In all regimes, the number of events is proportional to the beam luminosity and weighted by the cross section [22]. The total unpolarized Compton cross section is

$$\sigma = \frac{2\pi r_e^2}{X} \left[ \frac{1}{2} + \frac{8}{X} - \frac{1}{2(1+X)^2} + \left( 1 - \frac{4}{X} - \frac{8}{X^2} \right) \log(1+X) \right]. \quad (8)$$

The values of  $\sigma$  vary between the classical limit  $X \rightarrow 0$  and the ultrarelativistic limit  $X \rightarrow \infty$  as

$$\begin{cases} \lim_{X \rightarrow 0} \sigma = \frac{8\pi r_e^2}{3} (1-X) = \sigma_T (1-X) \\ \lim_{X \rightarrow \infty} \sigma = \frac{2\pi r_e^2}{X} \left( \log X + \frac{1}{2} \right), \end{cases} \quad (9)$$

where  $r_e$  is the classical electron radius, and  $\sigma_T = 0.67$  barn is the total Thomson cross section [23]. In particular, when the recoil factor is very large the relationship

$X = (E_{cm}/mc^2)^2$  holds, so the cross section scales roughly like the inverse square of the center of mass energy, i.e.,

$$\lim_{X \rightarrow \infty} \sigma \simeq (E_{cm}/mc^2)^2 [0.5 + \log(E_{cm}/mc^2)^2], \quad (10)$$

decreasing the probability to undergo Compton scattering between the incoming electron and the incident photon. Nevertheless, as extensively discussed in Ref. [5], the angular cross section peaks at  $\theta = 0$ , implying that the most likely scattering is backscattering of the photon, condition of maximum energy/momentum exchange between the electron and the photon, in which the values reported in Table I correspond. This may be the peculiarity of Compton scattering with respect to other two-particle interaction, like for example, Bhabha scattering or Moeller scattering, as is well shown in the evolution of the spectral distribution visible from Figs. 4–6.

### III. DEEP RECOIL AND SYMMETRIC COMPTON SCATTERING CANCEL ALL ANGULAR CORRELATIONS

All radiation emission by relativistic charged particles that involves a blueshift based on relativistic Doppler effect is characterized by an angular correlation of the emitted photon energy versus the angle of emission with respect to the propagation axis of the emitting particle. This is represented in all formulas by the well known  $\gamma^2 \theta^2$  term present in synchrotron radiation, ICS, betatron radiation, etc. Photons emitted at a nonzero  $\theta$  angle are redshifted with respect to that emitted at  $\theta = 0$ . On the other side, the radiation emission is concentrated within a  $\theta = 1/\gamma$  cone. It is only SYCS that cancels completely such an angular correlation. We rewrite Eq. (4) by expressing the formula only in terms of the recoil parameter  $X$ , the asymmetry factor  $A$ , and the Lorentz factor  $\gamma$ .  $A$  is generally defined, for any value of the electron velocity  $\beta$  and Lorentz factor  $\gamma$  as  $A = \beta\gamma^2 - X/4$ . We obtain

$$E'_{\text{ph}} = \frac{\gamma^2 + A + X/4}{\gamma^2 - A \cos \theta + X/4} E_{\text{ph}} \quad (11)$$

that is at all equivalent to Eq. (4). Stating that at the SYCS transition point ( $A = 0$ ), the dependence of the backscattered photon energy  $E'_{\text{ph}}$  on the scattering angle  $\theta$  is canceled (see Ref. [5] for further discussion). While SYCS truly cancels the angular correlation with the scattering angle, any large recoil regime  $X \gg 1$  is characterized by a strong damping of the angular correlation  $\gamma^2 \theta^2$ . We can rewrite Eq. (4) by assuming both  $\gamma \gg 1$  and  $\theta < 1/\gamma$  (see Ref. [14]) as

$$E'_{\text{ph}} = \frac{4\gamma^2 E_{\text{ph}}}{1 + \gamma^2 \theta^2 + X} \quad (12)$$

that can be asymptotically expressed for large values of  $X \gg 1$  as

$$E'_{\text{ph}} \simeq E_e \left( 1 - \frac{1 + \gamma^2 \theta^2}{X} \right) \quad (13)$$

clearly showing the damping of angular correlation at large recoils. As extensively discussed in Refs. [14] and [5], such a damping applies also to the angular spread at collision due to the electron beam emittance, making a deep recoil ICS insensitive to beam emittance, a great advantage in designing ICS sources for very monochromatic x and  $\gamma$  rays.

Another interesting effect of the large recoil regime is the cancellation of the dependence of backscattered photon energy on the collision angle. This is another quite surprising effect that can be appreciated by recalling the general formula (see, for instance, [24]):

$$E'_{\text{ph}} = E_{\text{ph}} \frac{\gamma^2 (1 - \beta \cos \alpha)}{\gamma^2 (1 - \beta \cos \theta) + \frac{X}{4} [1 - \cos(\alpha + \theta)]} \quad (14)$$

that reduces to Eq. (4) when the collision angle  $\alpha$  is equal to  $\alpha = \pi$ , i.e., at head-on collision.

When the recoil factor is very large, the previous formula asymptotically tends to

$$E'_{\text{ph}} \simeq \frac{4\gamma^2 E_{\text{ph}} (1 - \cos \alpha)/2}{1 + \gamma^2 \theta^2 + X(1 - \cos \alpha)/2}. \quad (15)$$

Considering photons fully backscattered at  $\theta = 0$  previous equation reduces to

$$E'_{\text{ph}} \simeq E_e \left( 1 - \frac{2}{X(1 - \cos \alpha)} \right) \quad (16)$$

clearly showing the desensitivity to collision angle  $\alpha$  induced by large recoils. From Eq. (16), it is indeed clear that, in large recoil condition, for all angles  $\pi/2 < \alpha < \pi$ , the correction to the photon energy introduced by the angle

is of order  $1/X$ . We have confirmed this with simulations. This peculiar property opens the way to designing sources of monochromatic gamma rays based on the interaction of monoenergetic low energy electron beams with photon hohlraums, where large x ray photon densities are stored (see Ref. [25]). If the electron-photon collision inside the hohlraum is taking place at large recoil values, then the energy of the secondary gamma-ray beam generated (leaving the hohlraum in the same direction of propagation of the electron beam) does not depend on the large dispersion of the collision angle inside the thermal x-ray photon bath. The dependence on the thermal photon energy spread is also canceled by large recoil interactions, through a spectral purification mechanism, as discussed in the next section.

#### IV. SPECTRAL PURIFICATION INDUCED BY DEEP RECOIL

The peculiar spectral behavior around the SYCS point can be exploited to conceive an extremely monochromatic source of  $\gamma$  rays. Starting from broadband radiation sources ( $\Delta E_{\text{ph}}/E_{\text{ph}} \simeq 30\%$ ), as channeling radiation [26] or betatron emission from plasma accelerated beams [27], a highly monochromatic gamma-ray beam can be produced by colliding these photons with electron beams of similar energy.

Once again large recoils reduce the dependence of the scattered photon beam bandwidth on the bandwidth of the incident photon beam, similar to what happens with angular correlations (as discussed in the previous section). Recalling that for large recoil factors  $X \gg 1$  the asymptotic expression of the backscattered photon at  $\theta = 0$  is given by  $E'_{\text{ph}} \simeq (1 - 1/X)E_e$ , we can easily derive the relative bandwidth of the backscattered photon beam  $\Delta E'_{\text{ph}}/E'_{\text{ph}}$  as

$$\frac{\Delta E'_{\text{ph}}}{E'_{\text{ph}}} \simeq \frac{1}{X} \frac{\Delta E_{\text{ph}}}{E_{\text{ph}}} \quad (17)$$

as a function of the incident photon beam relative bandwidth  $\Delta E_{\text{ph}}/E_{\text{ph}}$ . In agreement with Ref. [14] as far as the condition  $X \gg 1$  is assumed.

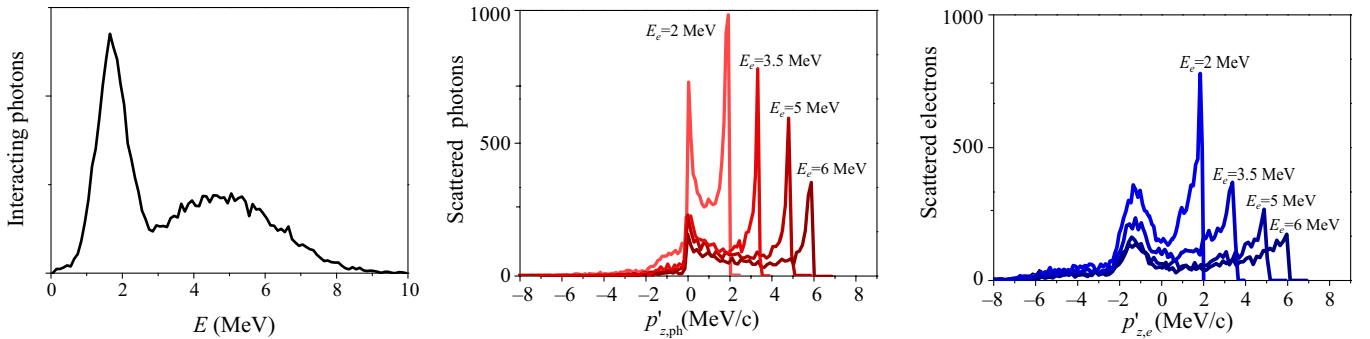


FIG. 8. Left window: Spectrum of the incident photon similar to channelling radiation in crystals, with colliding electron beams of energy  $E_e = 2, 3.5, 5,$  and  $6$  MeV. Central window: Momentum spectrum of scattered photons. Right window: Momentum spectrum of scattered electrons.

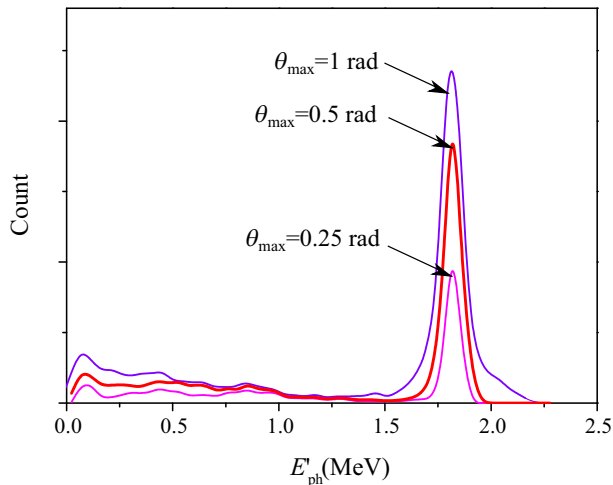


FIG. 9. Collimated energy spectrum.  $E_e = 1.9$  MeV, curve magenta:  $\theta_{\max} = 0.25$  rad, red:  $\theta_{\max} = 0.5$  rad, blue:  $\theta_{\max} = 1$  rad.

This damping of the incident photon beam bandwidth, which is compressed by a factor  $1/X$  into the backscattered photon beam bandwidth, is very clearly illustrated in Fig. 8, showing the initial energy spectrum (left window) and the emitted photon (central window) and electron (right window) momentum spectra, for the case of an incident broadband photon beam generated by channeling radiation in a crystal (Ref. [26]) and a colliding monoenergetic electron beam with variable energy, spanning the 2–6 MeV energy range. The photon beam spectra with a highly monochromatic peak shown in the central diagram clearly demonstrate the spectral purification mechanism enabled by the deep recoil inverse Compton scattering regime. Here what matters to achieve spectral purification is just a large value of the recoil factor  $X$ , which vary in a range from 64 (minimum value at 2 MeV colliding electron beam) up to about 200 (maximum value in case of 6 MeV electrons). The very peculiar point is that this example of the beam collision spans several regions of ICS, since the electron beam Lorentz factor  $\gamma$  varies from about 5 up to nearly 12, implying that the 2 MeV case is fully in RDSC regime, while 3.5 MeV is spanning across RDSC, SYCS, and EBS, 5 MeV covers EBS and FICS, and 6 MeV FICS and DRCS. As a consequence, the spectrum of the electron momentum (Fig. 8, right window) resembles the initial photon spectrum, but at the turn of the zero with an electron ensemble going forward and another going backward. No matter what regime is in action, as far as the recoil factor  $X$  is a large number, high spectral purification applies. Figure 9 presents instead the collimated energy spectrum, taken by selecting the radiation inside the angles  $\theta_{\max} = 0.25$  rad ( $\approx 1/\gamma$ ),  $\theta_{\max} = 0.5$  rad,  $\theta_{\max} = 1$  rad, where the spectral purification manifests itself evidently. Let us also underline the great advantage of using these deep recoil regimes to generate highly monochromatic gamma rays; the energy of the colliding electron beam

needed to generate gamma-ray beams in the MeV energy range is not much larger than a few MeV, unlike typical ICS sources aimed at gamma-ray beam generation in the ITS regime [28] where GeV-class electron beams are needed to enable applications in the photonuclear physics and photonics. Compactness and sustainability are certainly in favour of the deep recoil regime.

## V. CONCLUSIONS

We revisited the kinematics of Compton scattering, the electron-photon interactions producing electrons and photons in the exit channel, covering the full range of energy/momenta distribution between the two colliding particles, with a dedicated view to statistical properties of secondary beams that are generated in beam-beam collisions. Starting from the Thomson inverse scattering, where electrons do not recoil and photons are backscattered to higher energies by a Lorentz boost effect (factor  $4\gamma^2$ ), we analyze three transition points, separating four regions. These are in sequence, given by increasing the electron recoil (numbers are for transition points and letters for regions): (a) Thomson backscattering, with a recoil factor  $X \ll 1$  (1) equal sharing of total energy in the exit channel between electron and photon (recoil factor  $X = 1$ ), (b) deep recoil regime where the bandwidth/energy spread of the two interacting beams are exchanged in the exit channel (here  $1 \ll X \ll 2\gamma$ ) (2) electron is stopped, i.e., taken down at rest in the laboratory system by colliding with an incident photon of  $mc^2/2$  energy and the recoil factor is  $X = 2\gamma$ , (c) electron backscattering region, where incident electron is backscattered by the incident photon, with a recoil  $2\gamma < X < 4\gamma^2$  (3) symmetric scattering, when the incident particles carry equal and opposite momenta, so that in the exit channel they are backscattered with same energy/momenta and  $X = 4\gamma^2$ , (d) Compton scattering (*à la* Arthur Compton, see Ref. [4]), where photons carry an energy much larger than the colliding electron energy, occurring when  $X > 4\gamma^2$ . For each region and/or transition point, we discussed the potential effects of interest in diverse areas, like generating monochromatic gamma ray beams in deep recoil regions with spectral purification, or possible mechanisms of generation and propagation of very high energy photons in the cosmological domain.

## ACKNOWLEDGMENTS

We acknowledge useful discussions with Laura Bandiera and Gianfranco Paterno.

- 
- [1] A. Einstein, Zur Elektrodynamik bewegter Körper, *Ann. Phys. (N.Y.)* **17**, 891 (1905).
  - [2] J.J. Thomson, *Recent Researches in Electricity and Magnetism* (Clarendon Press, Oxford, 1893).

- [3] H. E. Ives and G. R. Stilwell, An experimental study of the rate of a moving atomic clock, *J. Opt. Soc. Am.* **28**, 215 (1938).
- [4] A. J. Compton, A quantum theory of the scattering of X-rays by light elements, *Phys. Rev.* **21**, 83 (1923).
- [5] L. Serafini, A. Bacci, C. Curatolo, I. Drebot, V. Petrillo, A. Puppini, M. R. Conti, and S. Samsam, Symmetric Compton scattering: A way towards plasma heating and tunable mono-chromatic gamma-rays, *Fundamental Plasma Phys.* **7**, 100026 (2023).
- [6] J. W. Follin Jr., Propagation of cosmic rays through interstellar space, PhD thesis, California Institute of Technology, Pasadena, CA, 1947.
- [7] E. Feenberg and H. Primakoff, Interaction of cosmic-ray primaries with sunlight and starlight, *Phys. Rev.* **73**, 449 (1948).
- [8] R. H. Milburn, Electron scattering by an intense polarized photon field, *Phys. Rev. Lett.* **10**, 75 (1963).
- [9] F. R. Arutyunian and V. A. Tumanian, The Compton effect on relativistic electrons and the possibility of obtaining high energy beams, *Phys. Lett.* **4**, 176 (1963).
- [10] O. F. Kulikov, Y. Y. Telnov, E. I. Filippov, and M. N. Yakimenko, Compton effect on moving electrons, *Phys. Lett.* **13**, 344 (1964).
- [11] C. Bemporad, M. Fotino, R. H. Milburn, and N. Tanaka, High-energy photons from Compton Scattering of light on 6.0-GeV electrons, *Phys. Rev.* **138**, B1546 (1965).
- [12] L. Federici, G. Giordano, G. Matone, G. Pasquariello, P. G. Picozza, R. Caloi, L. Casano, M. P. De Pascale, M. Mattioli, E. Poldi, C. Schaerf, M. Vanni *et al.*, Backward Compton scattering of laser light against high-energy electrons: The LADON photon beam at Frascati, *Il Nuovo Cimento B Series* **59**, 247 (1980).
- [13] N. Ranjan, B. Terzić, G. A. Krafft, V. Petrillo, I. Drebot, and L. Serafini, Simulation of inverse Compton scattering and its implications on the scattered linewidth, *Phys. Rev. Accel. Beams*, **21**, 030701 (2018).
- [14] C. Curatolo, I. Drebot, V. Petrillo, and L. Serafini, Analytical description of photon beam phase spaces in inverse Compton scattering sources, *Phys. Rev. Accel. Beams*, **20**, 080701 (2017).
- [15] P. Tomassini, A. Bacci, J. Cary, M. Ferrario, A. Giulietti, D. Giulietti, L. A. Gizzi, L. Labate, L. Serafini, V. Petrillo, and C. Vaccarezza, Linear and nonlinear Thomson scattering for advanced X-ray sources in PLASMONX, *IEEE Trans. Plasma Sci.* **36**, 1782 (2008).
- [16] V. Petrillo, I. Drebot, M. Ruijter, S. Samsam, A. Bacci, C. Curatolo, M. Opromolla, M. Rossetti Conti, A. R. Rossi, and L. Serafini, State of the art of high-flux Compton/Thomson X-rays sources, *Appl. Sci.* **13**, 752 (2023).
- [17] T. Akagi, A. Kosuge, S. Araki, R. Hajima, Y. Honda, T. Miyajima, M. Mori, R. Nagai, N. Nakamura, M. Shimada, T. Shizuma, N. Terunuma, and J. Urakawa, Narrow-band photon beam via laser Compton scattering in an energy recovery linac, *Phys. Rev. ST Accel. Beams*, **19**, 114701 (2016).
- [18] C. Bamber, S. J. Boege, T. Koffas, T. Kotseroglou, A. C. Melissinos, D. D. Meyerhofer, D. A. Reis, W. Raggi, C. Bula, K. T. McDonald, E. J. Prebys, D. L. Burke, R. C. Field, G. Horton-Smith, J. E. Spencer, D. Walz, S. C. Berridge, W. M. Bugg, K. Shmakov, and A. W. Weidemann, Studies of nonlinear QED in collisions of 46.6 GeV electrons with intense laser pulses, *Phys. Rev. D* **60**, 092004 (1999).
- [19] S. Vernetto and P. Lipari, Absorption of very high energy gamma rays in the Milky Way, *Phys. Rev. D* **94**, 063009 (2016).
- [20] H. Burkhardt and B. Pietrzyk, Low energy hadronic contribution to the QED vacuum polarization, *Phys. Rev. D* **72**, 057501 (2005).
- [21] C. Curatolo and L. Serafini, Electrons and X-rays to Muon Pairs (EXMP), *Appl. Sci.* **12**, 3149 (2022).
- [22] O. Klein and Y. Nishina, Über die Streuung von Strahlung durch freie Elektronen nach der neuen relativistischen Quantendynamik von Dirac., *Z. Phys.* **52**, 853 (1929).
- [23] J. D. Jackson, *Classical Electrodynamics*, 1st ed. (John Wiley & Sons, New York, 1962), ISBN 0-471-43131-1. OCLC 705218816.
- [24] I. Drebot, V. Petrillo, and L. Serafini, Two-colour X-gamma ray inverse Compton back-scattering source, *Europhys. Lett.* **120**, 14002 (2017).
- [25] O. J. Pike, F. Mackenroth, E. G. Hill, and S. J. Rose, A photon-photon collider in a vacuum hohlraum, *Nat. Photonics* **8**, 434 (2014).
- [26] U. I. Uggerhøj, The interaction of relativistic particles with strong crystalline fields, *Rev. Mod. Phys.* **77**, 1131 (2005).
- [27] A. Frazzitta, A. Bacci, A. Carbone *et al.*, First simulations for the EuAPS betatron radiation source: A dedicated radiation calculation code, *Instruments* **7**, 52 (2023).
- [28] EuroGammaS: Technical Design Report for the ELI-NP Gamma beam System, arXiv:1407.3669, 2014.